Spectral derivative based image reconstruction provides inherent insensitivity to coupling and geometric errors

Heng Xu, Brian W. Pogue, Roger Springett, and Hamid Dehghani

Thayer School of Engineering, Dartmouth College, Hanover, New Hampshire 03755

Received March 28, 2005; revised manuscript received June 16, 2005; accepted June 20, 2005

A reconstruction algorithm for multiwavelength diffuse optical tomography is presented, where instead of using data at each wavelength separately or even simultaneously, the difference in data for multiple wavelength pairs is used to reconstruct absolute concentration maps of chromophores. The results indicate a dramatic improvement in image reconstruction and the elimination of image artifacts, which are often associated with unknown measurement errors such as coupling coefficients and external boundary variations, because these errors are often less dependent on wavelength, and are effectively removed from the data set of the first derivative of intensity with respect to wavelength. © 2005 Optical Society of America

OCIS codes: 170.3010, 170.6960, 170.6510.

The fundamental limitation of diffuse optical tomography (DOT) has always been related to the diffuse nature of light passing through tissue, making the measured light a nonlinear function of both absorption and scattering properties of the medium as well as the exterior boundary of the tissue. This nonlinear transport leads to a hypersensitivity to the boundary, and small errors in measurement can significantly degrade performance by introducing artifacts within the reconstructed images. Errors such as coupling coefficient, boundary reflection mismatch, and inaccurate geometric modeling (i.e., of optical fiber positions) always exist and are unpredictable even in a reasonably well-calibrated system. Although corrections have been suggested,[1,2] the fundamental problem that these errors are easily coupled with the signals of interest is still a major limitation of most imaging systems. Image reconstruction algorithms that rely on absolute transmission data are sensitive to these errors because their objectives are to match the model-calculated data with the calibrated measurement data. Recently spectral reconstruction algorithms that allow direct chromophore and scattering reconstruction (DCSR) have been introduced.[3,4] Compared with the original indirect reconstruction method, which first reconstructs maps of the absorption coefficient (μ_a) and the reduced scattering coefficient (μ_s') at individual wavelengths, this method has shown improved accuracy and is more robust in the presence of noise, since it uses the coupled spectral information to constrain the reconstruction. However, currently described spectral methods rely on absolute spectrum measurement, and therefore those errors that are not common to all the optical fibers may introduce artifacts within the reconstructed parameters. In this Letter a novel reconstruction method is proposed that is inherently insensitive to fiber coupling errors, boundary reflection mismatch, and geometric modeling errors, allowing better spatial resolution and quantitative accuracy. The proposed algorithm is incorporated into a near-infrared (NIR) reconstruction algorithm.

For the proposed algorithm, the spectral derivative image reconstruction (SDIR) uses a difference of wavelengths in the DCSR approach, where the reconstruction algorithm minimizes the difference between the calculated and the measured first derivative of the spectrum. The algorithm presented is limited to the first-order approach to finite differencing for simplicity but may be used with higher-order approaches. Errors due to fiber and tissue coupling or external boundaries have a broadband offset effect that is largely wavelength independent. Therefore, by taking the difference at two adjacent wavelengths, these common errors are canceled and the remaining signal still contains the required information regarding the internal properties being imaged. This is similar to the concept of differential imaging approaches based on wavelength or temporal difference presented in Refs. 5 and 6. In those studies changes of absorption maps were reconstructed. The method proposed here reconstructs absolute concentration maps without relying on temporal data.

Based on the concept of DCSR, the direct and explicit reconstruction parameters become the scattering amplitude (a), the scattering power (b), the chromophore concentrations (hemoglobin [HbR], oxyhemoglobin [HbO_2], and water [H_2O]), and the indirect and implicit parameters μ_a and μ_s' and are not directly calculated.[4] Using this approach, a natural extension is to utilize spectral data types that minimize the effect of edge or coupling losses while preserving the spectral measurement of the interior, such as the first derivative of the spectrum.

The general DOT reconstruction algorithm is based on a standard least-squares error optimization. This is a minimization: $\Psi_0 = \|\Phi_{\lambda_1}{}^c(\mathbf{x}) - \Phi_{\lambda_1}{}^o\|_2{}^2$, where column vectors $\Phi_{\lambda_1}{}^c$ and $\Phi_{\lambda_1}{}^o$ represent calculated and measured fluence at all the source–detector pairs at wavelength λ_1. Vector x is the unknown parameter and is the spatially distributed optical properties, $x = [\mu_a(\lambda_1)\mu_s'(\lambda_1)]$. The DSCR method is based on two principles.[3] First, the wavelength-dependent absorp-

0146-9592/05/212912-3/$15.00

tion is a linear combination of each component, $\mu_a(\lambda)=\Sigma_i \epsilon_i(\lambda)c_i$, where ϵ_i is the specific extinction coefficient and c_i is the concentration map of the ith chromophore. Only three chromophores, HbR (c_1), HbO_2 (c_2), and H_2O (c_3), are considered in this work. Second, the wavelength dependence of reduced scattering is modeled by an empirical approximation to Mie theory, $\mu_s'(\lambda)=a(\lambda/\lambda_0)^{-b}$, where λ_0 is a reference wavelength, $\lambda_0=1$ μm is used in this work. The unknown parameters $x=[a\ b\ c_1\ c_2\ c_3]$ are independent of λ, and therefore measurements at multiple wavelengths can be combined to yield a new objective function:

$$\Psi_1=\|\Delta\Phi^{c-o}\|_2^2=\left\|\begin{Bmatrix}\Phi_{\lambda_1}{}^c(x)\\ \Phi_{\lambda_2}{}^c(x)\\ \vdots\\ \Phi_{\lambda_m}{}^c(x)\end{Bmatrix}-\begin{Bmatrix}\Phi_{\lambda_1}{}^o\\ \Phi_{\lambda_2}{}^o\\ \vdots\\ \Phi_{\lambda_m}{}^o\end{Bmatrix}\right\|_2^2. \quad (1)$$

The iterative formula for converging to a solution can be derived as $\Delta x=(\mathfrak{J}^T\mathfrak{J})^{-1}\mathfrak{J}^T\Delta\Phi^{c-o}$, where $\mathfrak{J}$ is the Jacobian matrix comprising the sensitivity for each parameter and the measurement at each wavelength:

$$\mathfrak{J}=[\mathfrak{J}_a\ \mathfrak{J}_b\ \mathfrak{J}_{c_1}\ \mathfrak{J}_{c_2}\ \mathfrak{J}_{c_2}]=\begin{bmatrix}\mathfrak{J}_{a,\lambda_1} & \mathfrak{J}_{b,\lambda_1} & \mathfrak{J}_{c_1,\lambda_1} & \mathfrak{J}_{c_2,\lambda_1} & \mathfrak{J}_{c_3,\lambda_1}\\ \mathfrak{J}_{a,\lambda_2} & \mathfrak{J}_{b,\lambda_2} & \mathfrak{J}_{c_1,\lambda_2} & \mathfrak{J}_{c_2,\lambda_2} & \mathfrak{J}_{c_3,\lambda_2}\\ \vdots & \vdots & \vdots & \vdots & \vdots\\ \mathfrak{J}_{a,\lambda_m} & \mathfrak{J}_{b,\lambda_m} & \mathfrak{J}_{c_1,\lambda_m} & \mathfrak{J}_{c_2,\lambda_m} & \mathfrak{J}_{c_3,\lambda_m}\end{bmatrix}. \quad (2)$$

In the SDIR approach, the objective function is modified from Eq. (1):

$$\Psi_2=\|\Delta\Phi'^{c-o}\|_2^2=\left\|\begin{Bmatrix}\Phi_{\lambda_1}{}^c(x)-\Phi_{\lambda_2}{}^c(x)\\ \Phi_{\lambda_2}{}^c(x)-\Phi_{\lambda_3}{}^c(x)\\ \vdots\\ \Phi_{\lambda_{m-1}}{}^c(x)-\Phi_{\lambda_m}{}^c(x)\end{Bmatrix}-\begin{Bmatrix}\Phi_{\lambda_1}{}^o-\Phi_{\lambda_2}{}^o\\ \Phi_{\lambda_2}{}^o-\Phi_{\lambda_3}{}^o\\ \vdots\\ \Phi_{\lambda_{m-1}}{}^o-\Phi_{\lambda_m}{}^o\end{Bmatrix}\right\|_2^2. \quad (3)$$

Here the prime denotes the finite difference operator to denote the similarity between the derivative and finite difference. The Jacobian matrix for SDIR can be easily derived from the Jacobian calculated using the conventional method and is the subtraction of the first $m-1$ row and the last $m-1$ row of $\mathfrak{J}$ in Eq. (2). The sequence of pairs of wavelengths used in Eq. (3) can be arbitrary; for example, one can use $\{[\lambda_1,\lambda_2],[\lambda_1,\lambda_3],\ldots\}$ or $\{[\lambda_1,\lambda_2],[\lambda_2,\lambda_3],\ldots\}$.

Questions remain as to whether SDIR can still provide sensitivity and specificity to resolve the chromophore and scattering properties accurately. Intuitively, in the derivative mode the common signals in the spectra are suppressed, thus more sensitive and independent sub-Jacobian matrices $(\mathfrak{J}_a,\mathfrak{J}_b,\mathfrak{J}_{c_1},\mathfrak{J}_{c_2},\mathfrak{J}_{c_3})$ can be constructed from the spectral contrast to provide better separation and localization of chromophore concentrations. This can be examined through the characteristics of the Jacobian matrix, such as the magnitude, rank, and cross correlation among sub-Jacobian matrices.[7] This choice of wavelength pairs is not critical when sufficient wavelengths are selected. Choosing wavelengths with a 20–40 nm gap is a convenient and effective strategy. However, to demonstrate the benefits and robustness of the SDIR algorithm, an example of the accuracy of the method is presented. One source and two symmetric detectors were used in a circular geometry to measure a homogeneous diffusive blood phantom with a broadband NIR tomography system.[8] Figure 1A shows the measured attenuation spectra (670–910 nm) at two symmetric detectors (D1, D2). Ideally, the spectra at the symmetric detectors for a symmetric and homogeneous phantom should overlap precisely, but in reality small differences are seen due to the different coupling coefficients as a function of the contact fibers and the phantom surface. Figure 1B shows the first-order difference spectra with a 20 nm wavelength gap. As can be seen, such differences are less wavelength dependent, which confirms the proposed idea of SDIR.

Simulations are provided to verify the merits of the new method by comparing the results with those of DCSR. We considered a 27 mm complex phantom with five distinct inclusions, as shown in Fig. 2A, where each inclusion had contrast for each given pa-

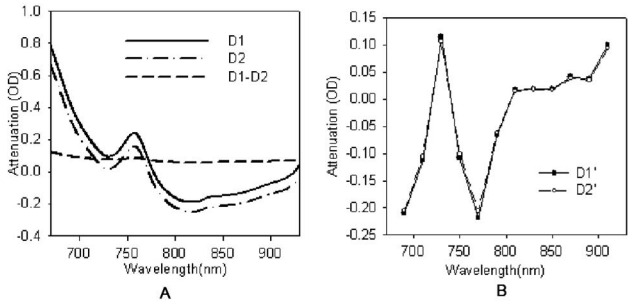

Fig. 1. A, Experiment geometry and source–detector fiber configuration. B, Measured attenuation spectra at D1, D2 and their difference. C, First-order finite difference spectra of D1 and D2 with a 20 nm separation.

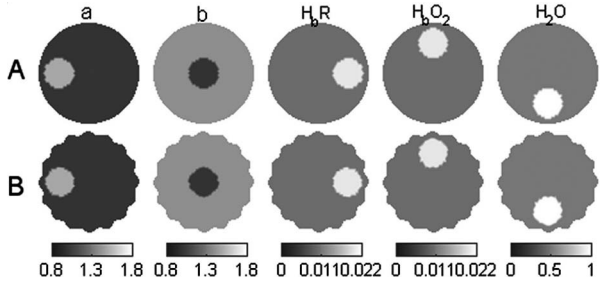

Fig. 2. A, Target phantom with five distinct inclusions (diameter=27 mm). Each column corresponds to the particular parameter. B, Target phantom for a simulation where an irregular boundary was considered.

Table 1. Properties of the Background Medium and Five Inclusions

	a	b	c_1(mM)	c_2(mM)	c_3
Background	1.0	1.4	0.01	0.01	0.5
Inclusions	1.5	1.0	0.02	0.02	1

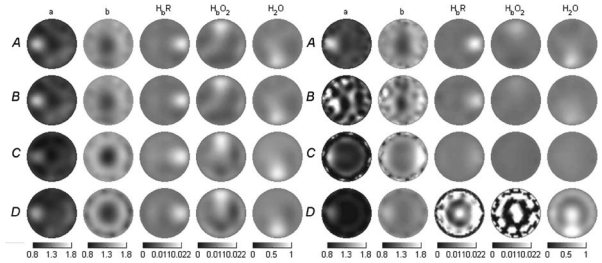

Fig. 3. A–D, Reconstructed images of simulations for both SDIR (left) and DCSR (right), with A, images having no data errors; B, 5% randomly distributed coupling errors; C, boundary reflection coefficient modeling error; D, reconstructing data taken from a distorted boundary shape.

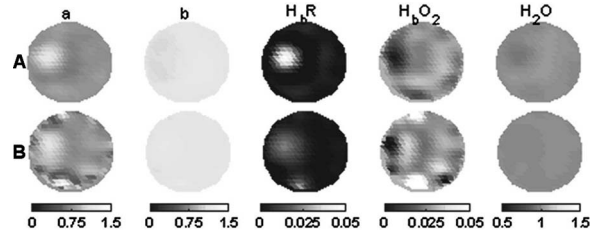

Fig. 4. Reconstructed images of a liquid phantom for both A, SDIR and B, DCSR. The background was 0.03 mM fully oxygenated blood with 1% Intralipid and the inclusion contained in a thin and clear straw was 0.09 mM fully deoxygenated blood with 2% Intralipid.

rameter. The background and the inclusion properties are listed in Table 1. Only the intensity measurement is considered. Measured data $\Phi_A{}^o$ at 13 wavelengths from 670 to 910 nm at every 20 nm were simulated by solving the diffusion equation by use of the finite-element method on a linear triangular mesh, having an equally distributed set of eight sources and eight detectors around the boundary. We added 0.5% Gaussian random noise to all synthesized data. Figure 3A shows the reconstruction of $\Phi_A{}^o$ by use of both SDIR and DCSR on the same mesh as the forward, therefore simulating a perfect model and data match. Figure 3B is the set of reconstructed images where 5% Gaussian coupling coefficient error was added to $\Phi_A{}^o$. Figure 3C shows a reconstruction in which the boundary reflection coefficient (relative reflective index $n_{\mathrm{rel}}=1.2$) was different from that used to generate $\Phi_A{}^o(n_{\mathrm{rel}}=1.4)$. Figure 3D shows a reconstruction in which geometric errors in modeling are considered by simulating the forward data on the irregular geometry shown in Fig. 2B [i.e., where fibers create a displacement (1 mm) on the tissue surface], but the reconstruction was still performed on the circular mesh.

As seen in Fig. 3, the original DCSR algorithm is sensitive to those errors that can introduce an error term into the absolute intensity measurement, and reconstructed artifacts are significant. Interestingly, the sources of error seem to have a distinct artifact pattern within each parameter channel. As expected, the SDIR algorithm shows a high tolerance to these errors and provides consistently more accurate reconstructions. In general, SDIR provides image qualities similar to those of the DCSR algorithm in the case where the error-free situation was used, as shown in Fig. 3A. In some channels, such as oxyhemoglobin, SDIR appears superior in terms of the reduction of parameter cross talk and quantitative accuracy. This is a direct result of the increased sensitivity for oxyhemoglobin within the differential spectrum.

An example of a series of liquid blood phantom experiments is shown in Fig. 4.[7] The inclusion separated from the background by a straw was connected to an external circulation to create different hemoglobin, oxygenation, or scattering contrast. Reconstructions for both methods were performed on the same calibrated dataset, but the SDIR outperformed the DCSR both qualitatively and quantitatively.

In conclusion, a novel approach to solve the DOT problem has been introduced. This method may help to overcome several major inherent measurement errors such as coupling coefficient variation, boundary reflection mismatch, and geometric mismodeling. The rationale is to use the difference or the derivative spectrum to cancel the common error term seen at each wavelength but also to maintain the scattering and chromophores spectral and spatial contrast. This method can be very useful in small animal and brain studies where fiber–tissue contact is more problematic but high spectral contrast is still available.

This work was sponsored by National Institutes of Health through grants NIH RO1 NS39471 and U54 CA105480. E-mail contact is Heng.Xu.th05@alum.dartmouth.edu or pogue@dartmouth.edu.

References

1. J. J. Stott, J. P. Culver, S. R. Arridge, and D. A. Boas, Appl. Opt. **42**, 3154 (2003).
2. J. Heino, E. Somersalo, and J. P. Kaipio, Opt. Express **13**, 296 (2005).
3. A. Corlu, T. Durduran, R. Choe, M. Schweiger, E. M. Hillman, S. R. Arridge, and A. G. Yodh, Opt. Lett. **28**, 2339 (2003).
4. S. Srinivasan, B. W. Pogue, S. Jiang, H. Dehghani, and K. D. Paulsen, Appl. Opt. **44**, 1858 (2005).
5. V. Ntziachristos, B. Chance, and A. G. Yodh, Opt. Express **5**, 230 (1999).
6. R. L. Barbour, H. L. Graber, Y. L. Pei, S. Zhong, and C. H. Schmitz, J. Opt. Soc. Am. A **18**, 3018 (2001).
7. H. Xu, "MRI-coupled broadband near-infrared tomography for small animal brain studies," Ph.D. dissertation (Dartmouth College, 2005).
8. H. Xu, R. Springett, H. Dehghani, B. W. Pogue, K. D. Paulsen, and J. F. Dunn, Appl. Opt. **44**, 2177 (2005).